Title	Predicting the solubilities of metal acetylacetonates in supercritical CO2: Thermodynamic approach using PC-SAFT
Author(s)	Ushiki, Ikuo; Fujimitsu, Ryo; Takishima, Shigeki
Citation	The Journal of Supercritical Fluids , 164 : 104909
Issue Date	2020-10-01
DOI	10.1016/j.supflu.2020.104909
Self DOI	
URL	https://ir.lib.hiroshima-u.ac.jp/00051509
Right	© 2020. This manuscript version is made available under the CC-BY-NC-ND 4.0 license http://creativecommons.org/licenses/by-nc-nd/4.0/ This is not the published version. Please cite only the published version. この論文は出版社版ではありません。引用の際には出版社版をご確認、ご利用ください。
Relation	

Predicting the solubilities of metal acetylacetonates in supercritical CO_2: Thermodynamic approach using PC-SAFT

Ikuo Ushiki, Ryo Fujimitsu, Shigeki Takishima*

Chemical Engineering Program, Graduate School of Advanced Science and Engineering, Hiroshima University, Kagamiyama, 1-4-1, Higashi-Hiroshima, Hiroshima 739-8527, Japan

*Corresponding author. E-mail: iushiki@hiroshima-u.ac.jp (I. Ushiki).

Abstract: Solubilities of metal precursors in supercritical carbon dioxide ($scCO_2$) are needed to effectively design the $scCO_2$-based deposition method. Herein, a method for predicting the solubilities of metal acetylacetonate (acac) precursors in $scCO_2$ was developed using the perturbed-chain statistical associating fluid theory (PC-SAFT) equation of state. Three PC-SAFT pure-component parameters viz., the segment diameter, segment number, and dispersion energy, for two metal acetylacetonates ($Cr(acac)_3$ and $Cu(acac)_2$) were determined by adjusting their values to the measured solubilities in organic solvents. The PC-SAFT parameters of $Cr(acac)_3$ and $Cu(acac)_2$ were then applied to predict the experimentally determined metal precursor solubilities in $scCO_2$ from the literature. The PC-SAFT predictions accurately described the experimental solubilities in $scCO_2$ over a wide range of pressures and temperatures even if the binary interaction parameter k_{ij} was set to 0. The isobaric solubilities in $scCO_2$ were also calculated with the generalized k_{ij} values, which provided a successful PC-SAFT description.

Keywords: Solubility; Supercritical carbon dioxide; PC-SAFT (perturbed-chain statistical associating fluid theory); Metal acetylacetonate; Prediction; Deposition

1. Introduction

Methods for depositing metals and metal oxides onto substrates using supercritical fluids as solvents, particularly supercritical carbon dioxide (scCO_2), have attracted increasing attention for preparing supported catalytic metal nanoparticles [1-9] and electronic devices [10-16]. The use of scCO_2 has several important advantages over conventional liquid-solvent methods, such as the solvent power for metal precursors, which can be tuned by adjusting the temperature and pressure, high diffusivity into the microstructure of the substrate, low surface tension, and not requiring a drying process [17, 18].

Dissolving a solid metal precursor in scCO_2 [17, 18] is the first step in deposition processes using scCO_2, and hence, quantifying the metal precursor solubilities is indispensable for designing these processes. Therefore, to date, solubility data for various metal precursors in scCO_2 have been experimentally obtained, e.g. metal acetylacetonate (acac) [19-26], cyclopentadienyl [22, 27], and heptanedionato [20, 21, 26] coordination complexes.

Contrarily, developing a theoretical model for predicting the metal precursor solubilities in scCO_2 is important for efficiently designing scCO_2-based deposition processes. Although semi-empirical models for describing metal precursor solubilities in scCO_2, such as the Chrastil equation [28], have been widely applied [22, 26, 29-31], determining the parameters of such models generally requires experimental solubility data of the target solute in scCO_2, which limits their predictive capability.

Models using the equations of state can be used to predict the solubilities of metal precursors in scCO_2. Cubic-type equations of state including the Peng–Robinson equation of state [32] are popular models based on the corresponding-state principle and critical properties (T_c and P_c). However, because the ligand structures of the metal precursors generally decompose at high temperatures, the critical points of metal precursors cannot actually exist; therefore, such cubic-type models are inappropriate for describing the solubilities of metal precursors in $scCO_2$.

Alternatively, statistical associating fluid theory (SAFT)-type equations of state based on molecular thermodynamics combined with perturbation theory [33-36] can be used to predict the solubilities of metal precursors in $scCO_2$. In particular, although several SAFT-type models have been proposed, the perturbed-chain (PC)-SAFT [37, 38] model has been widely applied because of its success in modeling asymmetric systems with complex molecules such as pharmaceuticals [39-41], polymers [42, 43], ionic liquids [44, 45], and deep eutectic solvents [46, 47], including under high-pressure conditions. However, to the best of our knowledge, the application of PC-SAFT for predicting the solubilities of metal precursors in $scCO_2$ has not been investigated in detail.

To describe the solubilities of metal precursors in $scCO_2$ using PC-SAFT calculations, three model parameters are necessary for each component i when there are no associating components that form hydrogen bonds in the target system, viz. the segment number m_i, the segment diameter σ_i, and the dispersion energy u_i. Generally, these three PC-SAFT parameters can be determined for each component by fitting the saturated liquid density and vapor pressure data of the pure component [37, 48], and in particular, the parameters for CO_2 have been determined using this method [37, 48]. However, because most metal precursors, including acac-type precursors, decompose at high temperatures [24], the PC-SAFT pure-component parameters for metal precursors are difficult to be determined using the physical properties of the pure components. Although our previous study [49] revealed that the PC-SAFT parameters of metal precursors can be used as adjustable parameters for fitting the solubilities of the metal acac precursors in $scCO_2$, this approach could not calculate the solubilities without using the fitting parameters. Paus et al. [50] and Ruether and Sadowski [51] previously determined the PC-SAFT pure-component parameters of various solid pharmaceuticals by fitting the PC-SAFT parameters to the solubilities of these compounds in various pure organic solvents, and they then predicted the solubilities of the solutes in water using the determined PC-SAFT pure-component parameters. A similar approach may be applied to determine the PC-SAFT pure-component parameters of metal precursors and predict their solubilities in $scCO_2$; however, this approach for predicting the solubilities of metal precursors in $scCO_2$ has not been reported to date.

Therefore, herein we aimed to develop a method for predicting the solubilities of metal acac precursors in $scCO_2$ using the PC-SAFT equation of state. We first measured the solubilities of metal acac precursors in various pure organic solvents. Then, we fit the solubility of the metal precursors in each pure organic solvent to the PC-SAFT model using the pure-component parameters as adjustable parameters. Finally, we employed the PC-SAFT model to predict the metal precursor solubilities in $scCO_2$ using the pure-component parameters determined by fitting the solubilities of the metal precursors in organic solvents.

2. Experimental

2.1 Materials

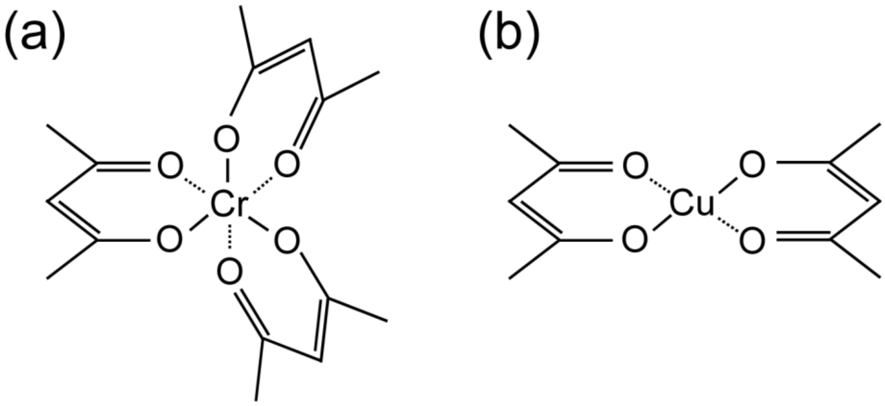

Figure 1. Molecular structures of (a) $Cr(acac)_3$ and (b) $Cu(acac)_2$.

Table 1. CAS number, supplier, and purity of the chemicals. Chemicals were used as-received.

Chemicals	CAS	Supplier	Purity [mass%]
$Cr(acac)_3$	21679-31-2	Sigma-Aldrich	99.9
$Cu(acac)_2$	13395-16-9	Sigma-Aldrich	99.9
Acetone	67-64-1	Nacalai Tesque	99.5
Toluene	108-88-3	Nacalai Tesque	99.8
Ethyl acetate	141-78-6	Nacalai Tesque	99.5
2-butanone	78-93-3	Nacalai Tesque	99.0

$Cr(acac)_3$ (chromium(III) acetylacetonate) and $Cu(acac)_2$ (copper(II) acetylacetonate) (Sigma-Aldrich, USA) were selected as the target metal precursors because reliable data for solubility in $scCO_2$ under a wide range of temperature and pressure conditions for these precursors have been published by Haruki et al. [19, 21, 23]. The molecular structures of these metal precursors are shown in **Figure 1**. Four organic solvents, namely, acetone, 2-butanone, toluene, and ethyl acetate (Nacalai Tesque, Japan), which are typical ketone, aromatic, and ester compounds, respectively, were selected as the solvents to dissolve the metal precursors.

All the chemicals were used as received without further purification, and their purities, CAS numbers, and suppliers are presented in **Table 1**.

2.2 Measuring the solubilities of metal precursors in organic solvents

The solubilities of the metal acac precursors in each organic solvent were measured based on the method used for solid pharmaceutical compounds reported by Paus et al [52]. An excess amount of the solid-state metal precursor was added to each pure organic solvent in a 200 cm^3 elementary flask, and the solution was mixed with a magnetic stirrer (Thermo Scientific, USA) at 500 rpm, atmospheric pressure, and a specific temperature controlled by a water bath (EYELA, Japan, SBC-16). The temperature of the solution in the elementary flask was measured using a calibrated platinum-resistance thermometer with an accuracy better than ±0.1 K. Erlenmeyer flasks containing the solvents were capped by a rubber stopper with a small hole (c.a. 3 mm), and the effect of water from the atmosphere on the solubility was assumed to be negligible because of the vapor generated from the organic solvent. After the system was maintained at a constant temperature for at least 24 h to ensure the thermodynamic equilibrium of dissolution, the magnetic stirrer was stopped for at least 30 min, and a small amount of the supernatant solution in the elementary flasks was sampled and diluted. The concentration of the solute in the supernatant was determined using a UV-vis spectrometer (U-3900H, Hitachi High-Tech Corp., Japan) at a wavelength of 330 nm based on pre-prepared calibration curves (the coefficient of determination R^2 was higher than 0.9995). Although a mass-based solubility measurement may be a much easier and efficient method, it is difficult to measure the mass of the metal precursor with adequate sensitivity because of its poor solubility in the organic solvents. Therefore, in this study, we employed the analytical method based on the UV-vis absorbance for measuring the metal precursor solubility. To convert the measured metal precursor concentration in grams per cubic decimeter to the corresponding mole fraction, the following equation for the temperature dependence of the solvent density for a saturated liquid was used [53]:

$$d_{\mathrm{s}}(T) = \frac{A}{B^{\left\{1+(1-T/C)^{D}\right\}}} \tag{1}$$

where $d_{\mathrm{s}}(T)$ is the solvent density (g/dm^3) at the temperature T (K), and A, B, C, and D are model parameters obtained from the literature [53, 54] (Table S1, Supplementary material). If the density of the metal precursor solution is assumed to be equal to the density of the pure solvent calculated using Eq. (1) owing to the low mole fraction of the metal acac precursors in the solvents, the mole fraction of the metal precursor in the solvent (x_{prec}) can be calculated as:

$$x_{\mathrm{prec}} = \frac{\dfrac{c_{\mathrm{prec}}}{M_{\mathrm{prec}}}}{\dfrac{c_{\mathrm{prec}}}{M_{\mathrm{prec}}} + \dfrac{d_{\mathrm{s}}(T)}{M_{\mathrm{s}}}} \tag{2}$$

where c_{prec} is the measured metal precursor concentration in the solvents (g/dm^3), and M_{prec} and M_{s} are the molar masses of the metal precursor and organic solvent, respectively.

The solubilities were measured at temperatures varying from 278 K to 303 K, which are lower than the boiling points of all the organic solvents and can be set using a water bath. At least two measurements were performed for each combination of the metal precursor and organic solvent, and the average values are reported as the experimental results. The relative combined expanded uncertainty U_{r} was estimated to be less than $U_{\mathrm{r}}(x_{\mathrm{prec}}) = 0.05$ with level of confidence being 0.95. Figure S1 (Supplementary material) shows the validation results of the solubility measurements using the reported solubilities of fluorene [55, 56] and anthracene [57, 58] in various organic solvents for temperature ranges similar to those used in our study. We used these solubility data owing to the lack of solubility data for the two metal acac precursors in organic solvents. The measured solubility values of these organic compounds in the solvents are evidently in good agreement with the literature data, validating the measurement method of the metal precursor solubility in the organic solvents used herein.

3. Model

3.1 PC-SAFT equation of state

In the PC-SAFT equation of state [37], the residual Helmholtz energy (a^{res}) of a system is calculated as the sum of different Helmholtz energy contributions that each depend on the physicochemical properties of the molecules [50]. These contributions are the hard-chain repulsion contribution a^{hc} and the dispersion (van der Waals) attraction contribution a^{disp}. Thus, the total residual Helmholtz energy is given by:

$$a^{\mathrm{res}} = a^{\mathrm{hc}} + a^{\mathrm{disp}} \tag{3}$$

Detailed expressions for these Helmholtz energy contributions are given in the literature [37]. For this work, the contribution of molecular association [38] is not considered in Eq. (3) because associating components that form hydrogen bonds are absent in the target systems. In such a non-associating system, the three PC-SAFT pure-component parameters required to describe a component i are the segment number m_i, the segment diameter σ_i, and the dispersion energy parameter u_i, which are usually determined by fitting to the vapor pressure and liquid density data of the corresponding pure component [37]. The methods used to determine these PC-SAFT parameters in this study are described in Section 3.2.

To describe a binary system, the conventional Lorentz–Berthelot combining rules are applied for a mixture of components i and j:

$$\sigma_{ij} = \frac{1}{2}\left(\sigma_i + \sigma_j\right) \tag{4}$$

and

$$u_{ij} = \left(1 - k_{ij}\right)\sqrt{u_i u_j} \tag{5}$$

To increase the accuracy of the model, the binary interaction parameter (k_{ij}) in Eq. (5) that describes the interactions between components *i* and *j* can be used as a fitting parameter in a fit to the experimental results if necessary [59].

3.2 Determining the PC-SAFT parameters by fitting to the solubility in the organic solvent

The values of the pure-component parameters (m_i, σ_i, and u_i) for all components present in the target system are necessary for the PC-SAFT calculation of the metal precursor solubilities in $scCO_2$. For CO_2, although there is some literature data on the PC-SAFT parameters, we employed the values reported by Diamantonis and Economou [48] (**Table 2**) because these PC-SAFT parameters, which were determined by fitting to the saturated vapor pressure and liquid density data of the pure component with higher accuracy, have been widely used for modeling high-pressure phase equilibria including CO_2 [60-63].

Table 2. Molar mass and PC-SAFT pure-component parameters for CO_2 and the organic solvents used in this work.

Component	M_i [g/mol]	m_i [-]	σ_i [Å]	u_i/k_B [K]	Ref.
CO_2	44.01	2.6037	2.555	151.04	[48]
Toluene	92.141	2.8149	3.7169	285.69	[37]
Ethyl acetate	88.106	3.5375	3.3079	230.80	[37]
Acetone	58.08	2.8913	3.2279	247.42	[64]
2-Butanone	72.11	2.9093	3.4473	260.07	[65]

As mentioned in the introduction, the PC-SAFT pure-component parameters for the metal acac precursors were determined by fitting the parameters to the solubilities of the metal precursors in various organic solvents. The PC-SAFT pure-component parameters of the organic solvents used in this study are listed in **Table 2**. Based on the thermodynamic phase equilibrium condition for the solid and liquid phases for which the chemical potentials of the metal precursor in both phases are equal, the metal precursor solubility in the organic solvent (x_{prec}) can be derived as [66-70]:

$$x_{\mathrm{prec}} = \frac{1}{\gamma_{\mathrm{prec}}} \exp\left\{ -\frac{\Delta h_{\mathrm{prec}}^{\mathrm{fus}}}{RT} \left(1 - \frac{T}{T_{\mathrm{m}}} \right) \right\} \tag{6}$$

where γ_{prec} is the activity coefficient of the metal precursor in the liquid phase, which consists of the dissolved metal precursor and the organic solvent. Although Eq. (6) is a very simple model for describing the solubilities of solid compounds in solvents and introducing Δc_{p} (the difference in the heat capacities of the solid and liquid metal precursor) can generally provide better results [71], we used this simplified version because there are no literature data of Δc_{p} and Eq. (6) has been widely applied to calculate the solubilities of solid pharmaceuticals in organic solvents [51, 67]. In Eq. (6), $\Delta h_{\mathrm{prec}}^{\mathrm{fus}}$ and T_{m} are the enthalpy of fusion and melting point of the solid metal precursors, respectively, and with the exception of $\Delta h_{\mathrm{prec}}^{\mathrm{fus}}$ for $Cu(acac)_2$, these parameters were obtained from the literature (**Table 3**). Because the value of $\Delta h_{\mathrm{prec}}^{\mathrm{fus}}$ for $Cu(acac)_2$ is not available in the literature, this parameter was also treated as an adjustable parameter in the fit to the solubility of the metal precursors in $scCO_2$ along with the three PC-SAFT parameters following the method reported by Ruether and Sadowski [51] for calculating the solubilities of pharmaceuticals in organic solvents. In using Eq. (6), it was assumed that the metal precursor does not dissociate in the solvent and dosed not change its solid form.

Table 3. Physical properties of the solid-state metal precursors

Metal precursors	$\Delta h_{\text{prec}}^{\text{fus}}$ [kJ/mol]	T_{m} [K]	$v_{\text{prec}}^{\text{solid}}$ [cm^3/mol]
$Cr(acac)_3$	35.9 [54]	486 [54]	257.1 [72]
$Cu(acac)_2$	44.6 [a]	509 [73]	164.2 [72]

a: Treated as an adjustable parameter in fitting of metal precursor-organic solvent solubility data

The activity coefficient γ_{prec} in Eq. (6) is defined as the ratio between the fugacity coefficients of the metal precursor in the solvent ($\varphi_{\text{prec}}^{\text{L}}$) and the pure metal precursor in liquid form ($\varphi_{0,\text{ prec}}^{\text{L}} = \varphi_{\text{prec}}^{\text{L}}\left(x_{\text{prec}} \rightarrow 1\right)$), as described by [50, 74]:

$$\gamma_{\text{prec}} = \frac{\varphi_{\text{prec}}^{\text{L}}}{\varphi_{0,\text{ prec}}^{\text{L}}} \tag{7}$$

The fugacity coefficients are calculated based on the corresponding residual chemical potential ($\mu_{\text{prec}}^{\text{res}}$):

$$\ln \varphi_{\text{prec}} = \frac{\mu_{\text{prec}}^{\text{res}}\left(T, V, x_{\text{prec}}\right)}{RT} - \ln Z \tag{8}$$

where T, V, and Z are the temperature, volume, and compressibility factor of the system, and x_{prec} is the mole fraction of the precursor in the solvent. $\mu_{\text{prec}}^{\text{res}}$ can be obtained from the partial derivative of the residual Helmholtz energy of the system (a^{res}) used in PC-SAFT (Eq. (3)) with respect to its mole fraction at constant T and V and is given by:

$$\frac{\mu_{\text{prec}}^{\text{res}}\left(T,V,x_{\text{prec}}\right)}{RT}=\frac{a^{\text{res}}}{RT}+\left(Z-1\right)+\left(\frac{\partial\left(a^{\text{res}}/RT\right)}{\partial x_{\text{prec}}}\right)_{T,V,x_{j\neq\text{prec}}}-\sum_{k=1}^{N}\left(x_k\left(\frac{\partial\left(a^{\text{res}}/RT\right)}{\partial x_k}\right)_{T,V,x_{i\neq k}}\right) \quad (9)$$

The detailed expressions for a^{res} and Z can be found in the original PC-SAFT report [37].

Thus, the solubilities of the metal precursors in each pure organic solvent were calculated using Eq. (6) and fitted to the corresponding experimental solubility data using the three PC-SAFT pure-component parameters (m_i, σ_i, and u_i) for the metal precursors as adjustable parameters while minimizing the average relative deviation (ARD) defined as:

$$\text{ARD}\left[\%\right]=\frac{1}{ND}\sum_{i}^{ND}\frac{\left|x_{\text{prec,calc},i}-x_{\text{prec,exp},i}\right|}{x_{\text{prec,exp},i}}\times 100 \quad (10)$$

In the fits used to determine the PC-SAFT pure-component parameters for the metal precursors, the binary interaction parameter k_{ij} in Eq. (5) was set to zero. The fitting calculations were performed using the simplex optimization method in MATLAB® 2019b.

3.3 Predicting the solubilities of metal precursors in scCO$_2$ by PC-SAFT

Based on the thermodynamic relationship expressed using the fugacities of the precursors in the solid and supercritical phases, the solubility of a metal precursor in scCO$_2$ (y_{prec}) can be modeled as [40, 49, 66, 75]:

$$y_{\text{prec}} = \frac{p_{\text{prec}}^{\text{sub}}}{P\varphi_{\text{prec}}^{\text{scf}}} \exp\left[\frac{v_{\text{prec}}^{\text{solid}}\left(P - p_{\text{prec}}^{\text{sub}}\right)}{RT}\right] \tag{11}$$

Here, $v_{\text{prec}}^{\text{solid}}$ is the solid molar volume of the metal precursor, which was taken from the literature [72], as shown in **Table 3**. In Eq. (11), $\varphi_{\text{prec}}^{\text{scf}}$ is the fugacity coefficient of the metal precursor in $scCO_2$, which can be calculated with PC-SAFT according to Eqs. (8) and (9) using the corresponding chemical potential with the pure-component parameters of each component, as described in section 3.2. $p_{\text{prec}}^{\text{sub}}$ is the sublimation pressure of the metal precursor, which was calculated by interpolating and extrapolating data from the literature (**Table 4**) with the Clausius–Clapeyron equation [76] as follows:

$$p_{\text{prec}}^{\text{sub}} = p_{\text{prec}}^{\text{sub}\,*} \exp\left[-\frac{\Delta h_{\text{prec}}^{\text{sub}}}{R}\left(\frac{1}{T} - \frac{1}{T^*}\right)\right] \tag{12}$$

where $\Delta h_{\text{prec}}^{\text{sub}}$ is the enthalpy of sublimation of the metal precursor, and $p_{\text{prec}}^{\text{sub*}}$ and T^* are the reference sublimation pressure and temperature, respectively (**Table 4**).

Table 4. Values of $\Delta h_{\text{prec}}^{\text{sub}}$, $p_{\text{prec}}^{\text{sub*}}$, and T^* for the metal precursors in Eq. (12).

Metal precursor	$\Delta h_{\text{prec}}^{\text{sub}}$ [kJ/mol]	$p_{\text{prec}}^{\text{sub*}}$ [Pa]	T^* [K]	Experimental T range [K]	Ref.
$Cr(acac)_3$	127.28	1.77×10^{-4}	320	320–476	[77]
$Cu(acac)_2$	115.10	2.31×10^{-4}	315	315–386	[78]

Thus, the method for predicting the solubility of a metal precursor in $scCO_2$ using PC-SAFT can be summarized as,

(i) The solubilities of the metal precursor in different pure organic solvents are measured.

(ii) PC-SAFT pure-component parameters (m_i, σ_i, and u_i) for the metal precursor are determined using fits to the measured solubility data of the metal precursor in the organic solvents.

(iii) The literature data of the metal precursor solubilities in $scCO_2$ are predicted using PC-SAFT, where k_{ij} is set to zero in Eq. (5), using the determined pure-component parameters of the metal precursor.

The ARD between the predicted and experimental values of the solubilities was calculated according to a formula similar to Eq. (10). In addition, the logarithm-based ARD ($\mathrm{ARD}^{\log}$) defined in Eq. (13) was also used to evaluate the predicted results of the solubilities in $scCO_2$.

$$\mathrm{ARD}^{\log}\ [\%] = \frac{1}{ND}\sum_{i}^{ND}\left|\frac{\ln y_{\mathrm{prec,calc},i} - \ln y_{\mathrm{prec,exp},i}}{\ln y_{\mathrm{prec,exp},i}}\right| \times 100 \tag{13}$$

4. Results and Discussion

4.1 Measuring and fitting the solubilities of metal precursors in organic solvents

4.1.1 Measured solubilities of metal precursors in organic solvents

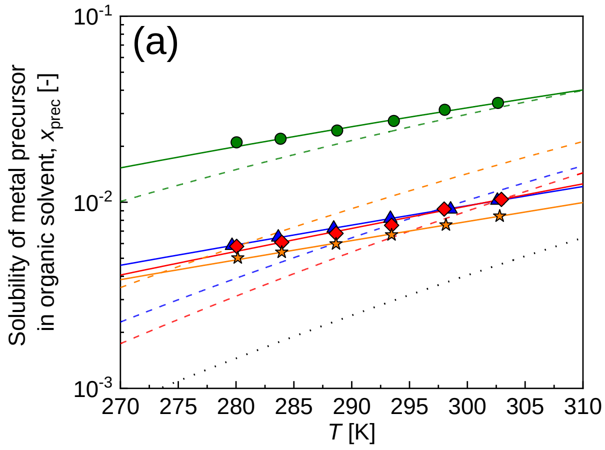

Figure 2. Measured solubilities of **(a)** $Cr(acac)_3$ and **(b)** $Cu(acac)_2$ in toluene (●), acetone (◆), ethyl acetate (▲) and butanone (★) with fits obtained with PC-SAFT at k_{ij} = 0 (dashed lines) using the pure-component parameters of the metal precursors as fitting parameters and additional fitting results using k_{ij} as an additional fitting parameter (solid lines). The dotted line indicates the ideal solubility of the metal precursor for γ_{prec} =1 in Eq. (6).

Figure 2(a) shows the measured $Cr(acac)_3$ solubilities in four pure organic solvents, viz., toluene, acetone, ethyl acetate, and butanone, and the obtained values are also listed in Table S2. **Figure 2**(a) reveals that $Cr(acac)_3$ solubility increased with increasing temperature, showing the typical temperature-dependent solubility of solid organic compounds in organic solvents at atmospheric pressure [79]. In the investigated temperature range, the $Cr(acac)_3$ solubilities follow the order of toluene > acetone ≈ ethyl acetate ≈ butanone. The higher solubility of this metal precursor in toluene is probably due to the higher affinity of the aromatic compound to the acac ligand (**Figure 1**).

Figure 2(b) shows the measured solubilities of $Cu(acac)_2$ in the pure organic solvents, showing a temperature dependence similar to that of $Cr(acac)_3$ in **Figure 2(a)**. In addition, $Cu(acac)_2$ was 1–2 orders of magnitude less soluble than $Cr(acac)_3$ in all four solvents. The acac ligands in the metal precursors (**Figure 1**) have a high affinity for the organic solvents, especially for toluene, as mentioned above. $Cu(acac)_2$ has two acac ligands, whereas $Cr(acac)_3$ has three, which explains why the solubility $Cu(acac)_2$ is lower. On the other hand, the solubilities $Cu(acac)_2$ in the four pure solvents follow the order of ethyl acetate > toluene > acetone ≈ butanone, thus showing a different trend from that for $Cr(acac)_3$. This difference may also be related to the different numbers of acac ligands in these two metal precursors. The organic solvent molecules interact more easily with the metal center of $Cu(acac)_2$ than with $Cr(acac)_3$ because the former has fewer acac ligands, giving rise to the difference between $Cr(acac)_3$ and $Cu(acac)_2$ for the order of the solubilities in the four pure organic solvents. However, experimental data for other metal precursors will be required to provide the detailed discussion about these results.

4.1.2 Results of fitting the solubilities of metal precursors in organic solvents

Table 5. Molar mass and PC-SAFT parameters for metal precursors investigated in this work.

Component	M_i [g/mol]	m_i [-][a]	σ_i [Å][a]	u_i/k_B [K][a]	ARD [%][b]
$Cr(acac)_3$	349.320	13.6814	3.0326	169.22	26.9
$Cu(acac)_2$	261.762	7.9551	3.6500	188.55	23.7

a: Treated as an adjustable parameter in fitting of metal precursor-organic solvent solubility data
b: Average relative deviation defined by Eq. (10) in the fitting for all data points for each metal precursor with k_{ij} in Eq. (5) set to zero.

The dashed lines in **Figure 2** correspond to the fitting results for the measured solubilities of the metal precursors in the different pure organic solvents when the three PC-SAFT pure-component parameters were used as the fitting parameters, while k_{ij} in Eq. (5) was set at zero. The PC-SAFT parameters of the metal precursors determined by the fitting are listed in **Table 5** together with the ARD values of the fits. As shown in **Figure 2** and **Table 5**, the PC-SAFT fits can approximately describe the trend in the solubilities of the metal precursors in the four solvents. Furthermore, **Table 5** indicates a reasonable trend for the PC-SAFT parameter m_i of the metal precursors, i.e. m_i increased with the increasing molar mass and number of acac ligands (**Figure 1**), as was previously reported for typical organic compounds [37, 68]. The higher values for the σ_i and u_i/k_B parameters with the lower number of acac ligands may be interpreted as due to the larger influence of the metal center in the precursor with fewer ligands; however, other metal precursors with different numbers of ligands must be investigated in detail to confirm the generality of this trend. Figure S2 shows the sensitivity of each PC-SAFT parameter for $Cr(acac)_3$ in the determination of the parameters by adjusting it to the solubilities of $Cr(acac)_3$ in pure solvents. In the validation of the sensitivity, the other PC-SAFT parameters were set to the optimized values (**Table 5**). Figure S2 reveals that the parameter σ_i of the metal precursor shows higher sensitivity in the calculation of the solubilities of metal precursors in the studied organic solvents in comparison with those of the other two parameters, m_i and u_i.

4.1.3 Additional fitting using k_{ij}

The temperature dependence of the fitted results shown by the dashed lines in **Figure 2** is different from that of the experimental results, and relatively large differences between the calculated and experimental solubilities are observed for some systems. This is likely because the interactions between the metal precursor and organic solvent described by the combining rule for the dispersion energies in Eq. (5) are not adequately considered in the PC-SAFT when k_{ij} is set to zero. Therefore, after fitting using the three PC-SAFT pure-component parameters, an additional fitting to the experimental solubility data using k_{ij} was performed for each metal precursor-solvent system using a temperature-dependent equation for k_{ij} that is suitable for evaluating the solubilities of solid pharmaceuticals in organic solvents [50, 52], as follows:

$$k_{ij} = k_{ij,\mathrm{slope}} T + k_{ij,\mathrm{intercept}} \tag{14}$$

Table 6. Binary interaction parameters (k_{ij}) for the interactions between metal precursors and solvents and ARDs between the fitted and experimental metal precursor solubilities obtained by the additional fitting, using k_{ij} as an adjustable parameter

Metal precursors	Solvent	$k_{ij,\mathrm{slope}} \times 10^4$ [K^{-1}][a]	$k_{ij,\mathrm{intercept}}$ [-][a]	ARD [%][b]
$Cr(acac)_3$	Toluene	1.272	−0.0396	1.8
	Ethyl acetate	2.829	−0.0840	0.3
	Acetone	2.572	−0.0779	2.6
	2-Butanone	2.903	−0.0794	0.7
	Overall			1.4
$Cu(acac)_2$	Toluene	3.601	−0.1043	0.7
	ethyl acetate	5.015	−0.1446	1.3
	Acetone	4.970	−0.1448	1.6
	2-butanone	4.353	−0.1255	0.8
	Overall			1.2

a: Parameter coefficients in Eq. (14).
b: ARD of the additional fitting to the experimental solubility data using k_{ij} as an adjustable parameter after the fitting using three PC-SAFT pure-component parameters.

The solid lines in **Figure 2** denote the results of PC-SAFT calculation using k_{ij} as an additional adjustable parameter in the fitting for the experimental solubilities after fitting using the three PC-SAFT pure-component parameters (dashed lines), while **Table 6** and Figure S3 show the k_{ij} values obtained by the fitting. The results presented in **Figure 2** and **Tables 5 and 6** demonstrate that unsurprisingly, the additional PC-SAFT fitting using k_{ij} significantly improved the accuracy of the fitting of the solubilities of metal precursors in the organic solvents.

4.2 Calculating the solubilities of metal precursors in scCO$_2$

4.2.1 Predicting the solubilities using PC-SAFT

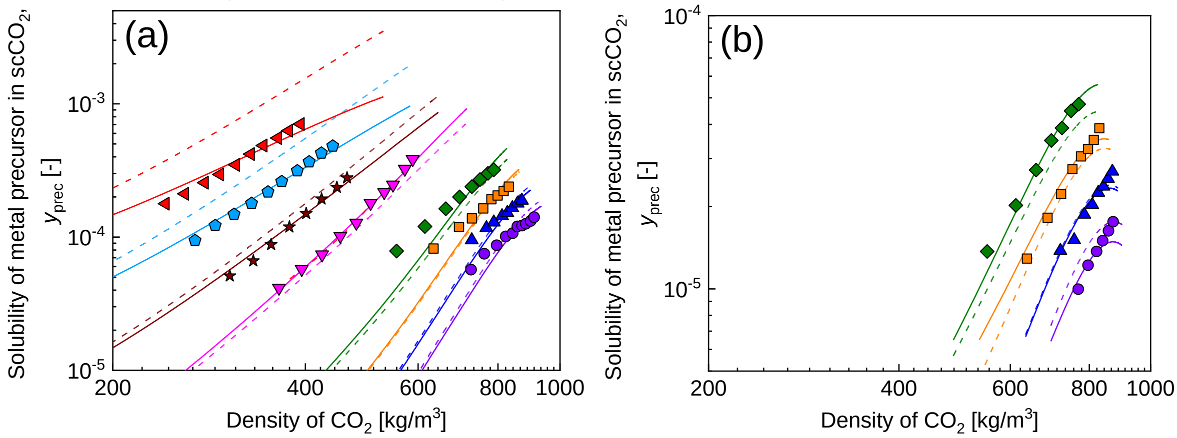

Figure 3. Isothermal solubilities of **(a)** Cr(acac)$_3$ and **(b)** Cu(acac)$_2$ in scCO$_2$ as a function of CO$_2$ density in the pressure range of 16.0 MPa to 30.3 MPa. Symbols: experimental values from the literature [19, 21, 23] at 433 K (◀), 413 K (⬟), 393 K (★), 373 K (▼), 343 K (◆), 333 K (■), 323 K (▲) and 313 K (●); dashed lines: PC-SAFT prediction with k_{ij} = 0; solid lines: PC-SAFT fit using k_{ij} as an adjustable parameter in Eq. (5).

Table 7. Predicted and fit results of the isothermal solubilities of the metal precursors in scCO$_2$ obtained using PC-SAFT at P = (16.0 to 30.3) MPa.

Metal precursors	T [K]	$\mathrm{ARD}_{\mathrm{pred}}$ [%][a]	$\mathrm{ARD}_{\mathrm{fit}}$ [%][b]	k_{ij} [-][c]	$\mathrm{ARD}^{\mathrm{log}}_{\mathrm{pred}}$ [%][d]	$\mathrm{ARD}^{\mathrm{log}}_{\mathrm{fit}}$ [%][e]
Cr(acac)$_3$	433	110.8	10.4	0.0460	9.5	1.3
	413	59.8	6.5	0.0250	5.6	0.8
	393	22.4	6.8	0.0088	2.2	0.7
	373	16.2	3.8	−0.0064	2.0	0.4
	343	25.4	18.0	−0.0039	3.6	2.4
	333	14.3	14.1	−0.0008	1.8	1.8
	323	11.2	9.7	0.0014	1.3	1.2
	313	15.8	12.4	0.0017	1.7	1.4
	overall	36.3	10.0	-	3.6	1.2
Cu(acac)$_2$	343	17.9	4.7	−0.0054	1.9	0.5
	333	7.9	2.7	−0.0018	0.8	0.3
	323	6.3	6.2	0.0005	0.6	0.6
	313	13.4	6.5	0.0034	1.1	0.6
	overall	11.0	4.8	-	1.1	0.5

a: Predicted deviation defined with Eq. (10) using PC-SAFT while k_{ij} in Eq. (5) is set to zero.
b: Deviation of the fits using PC-SAFT with k_{ij} as an adjustable parameter at each temperature with Eq. (10) as the objective function.
c: Binary interaction parameter between CO$_2$ and metal precursor determined by fitting.
d: Predicted deviation defined with Eq. (13) using PC-SAFT while k_{ij} in Eq. (5) is set to zero.
e: Deviation of the calculated values defined with Eq. (13) using PC-SAFT with the k_{ij} values.

The dashed lines in **Figure 3** show the predicted isothermal solubilities of $Cr(acac)_3$ [19, 23] and $Cu(acac)_2$ [21] in $scCO_2$ as a function of the CO_2 density [80] using PC-SAFT and pure-component parameters of the metal precursors (**Table 5**) determined by fitting to the solubilities in the organic solvents, as mentioned in section 4.1.2. **Table 7** summarizes the ARD values obtained by comparing the experimental and predicted results. As shown by the dashed lines in **Figure 3** and the data presented in **Table 7**, the PC-SAFT predictions reproduced the isothermal solubilities of the metal precursors in $scCO_2$ with ARD values defined by Eq. (10) being less than 26% for almost all of the investigated conditions, even though k_{ij} was set at 0 in the combining rule (Eq. (5)). Figure S4 shows the effect of each PC-SAFT parameter for $Cr(acac)_3$ on the prediction of the metal precursor solubilities in $scCO_2$. For the validation of the sensitivity, the PC-SAFT parameters were maintained the same as those used to obtain the data in Figure S2, and the other parameters were set to the optimized values determined by adjusting them to the solubilities in organic solvents (**Table 5**). Figure S4 reveals that the PC-SAFT parameter determined by fitting the solubilities in organic solvents is suitable for predicting the solubilities in $scCO_2$. In addition, **Table 7** also includes the logarithm-based ARD (ARD^{log}) defined with Eq. (13), which indicates a similar trend to that of the standard ARD defined by Eq. (10), although the ARD^{log} values were less than the ARD values by one order of magnitude.

4.2.2 Calculating the solubilities using k_{ij}

As shown in **Figure 3** and **Table 7**, a particularly large deviation is observed in the predicted solubilities of $Cr(acac)_3$ at higher temperatures when k_{ij} = 0. Therefore, additional PC-SAFT calculations were performed using k_{ij} in Eq. (5) as an adjustable parameter for each temperature and precursor condition. The solid lines in **Figure 3** show the fitting results for the metal precursor solubilities in $scCO_2$, and **Table 7** lists the corresponding k_{ij} values and the fitting ARD values. The results in **Figure 3** and **Table 7** indicate that when k_{ij} is introduced as an additional fitting parameter, the PC-SAFT calculations accurately describes the dependence of the solubilities on the CO_2 density to the ARD within 18% for all investigated conditions.

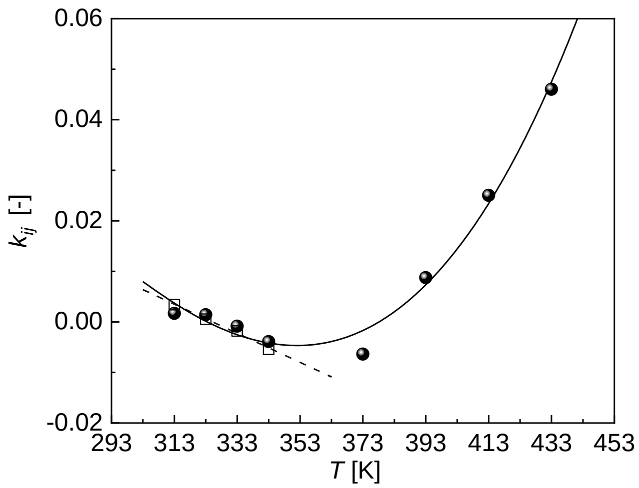

Figure 4. Temperature dependence of k_{ij} (**Table 7**) in the combining rule (Eq. (5)), determined by fitting to the solubility data for Cr(acac)$_3$ (●, solid line: Eq. (15)) and Cu(acac)$_2$ (☐, dashed line: Eq. (16)) using PC-SAFT.

Figure 4 shows the temperature dependence of the k_{ij} values (**Table 7**) used in the combining rule (Eq. (5)), determined by the PC-SAFT fitting to the solubility data for Cr(acac)$_3$ and Cu(acac)$_2$ in $scCO_2$ at each temperature. Over the temperature range of 313 K to 373 K, k_{ij} values for both Cr(acac)$_3$ and Cu(acac)$_2$ decreased with increasing temperature; considering the physical meaning of Eq. (5), this trend implies that the energy of the interaction between the metal precursor and CO_2 increased with increasing temperature under conditions of lower temperature but higher CO_2 density. On the other hand, as shown in **Figure 4**, the k_{ij} value for Cr(acac)$_3$ increased significantly above 373 K; this finding can be attributed to the decreasing CO_2 density with increasing temperature, which may weaken the interactions between CO_2 and Cr(acac)$_3$ at higher temperatures.

Using the least-squares method, the temperature dependence of the k_{ij} values for each metal precursor and CO_2 can be fit to the following polynomials:

$$\mathrm{Cr(acac)_3}: \; k_{ij} = aT^3 + bT^2 + cT + d \tag{15}$$

$$\mathrm{Cu(acac)_2}: k_{ij} = cT + d \tag{16}$$

where *a*, *b*, *c*, and *d* are the coefficients used in the fits (**Table 8**).

Table 8. Coefficients for Eqs. (15) and (16).

Metal precursors	$a \times 10$ [K^{-3}]	$b \times 10^5$ [K^{-2}]	$c \times 10^3$ [K^{-1}]	d [-]	R^2[-] [a]
$Cr(acac)_3$: Eq. (15)	2.0291	−1.5121	3.1011	−0.1078	0.984
$Cu(acac)_2$: Eq. (16)	-	-	−0.2877	0.0935	0.993

a: Coefficient of determination in the least-squares method

The solid and dashed lines in **Figure 4** denote the results for $Cr(acac)_3$ and $Cu(acac)_2$, respectively, obtained for k_{ij} using Eqs. (15) and (16), demonstrating that the generalized k_{ij} equation can describe the observed temperature dependence of this parameter.

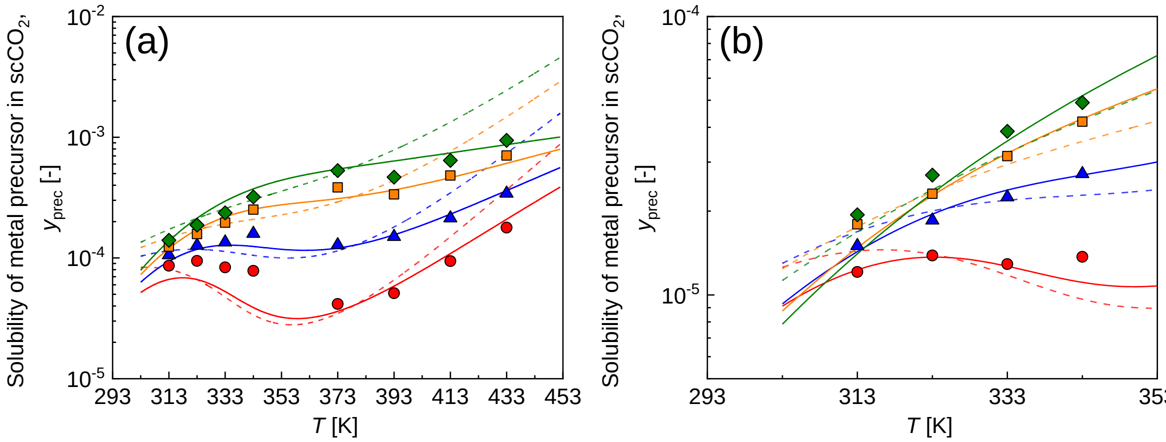

Figure 5. Isobaric solubilities of **(a)** $Cr(acac)_3$ and **(b)** $Cu(acac)_2$ in $scCO_2$ as a function of temperature. Symbols: experimental data determined by interpolating and extrapolating from the literature values [19, 21, 23] at 30.0 MPa (◆), 25.0 MPa (■), 20.0 MPa (▲), and 16.0 MPa (●); dashed lines: PC-SAFT predictions with k_{ij} = 0; solid lines: PC-SAFT calculation with generalized k_{ij} obtained using Eqs. (15) and (16).

Table 9. Calculated results of the isobaric solubilities of the metal precursors in $scCO_2$ obtained using PC-SAFT at T = (313 to 433) K.

Metal precursors	P [MPa]	ARD_{pred} [%][a]	ARD_{calc} [%][b]
$Cr(acac)_3$	30.0	48.6	14.4
	25.0	33.6	8.4
	20.0	34.3	8.7
	16.0	43.2	25.0
	overall	39.9	14.1
$Cu(acac)_2$	30.0	14.8	6.0
	25.0	9.5	3.5
	20.0	6.2	7.0
	16.0	14.3	14.8
	overall	11.2	7.8

a: Predicted deviation defined with Eq. (10) using PC-SAFT while k_{ij} in Eq. (5) is set to zero.
b: Calculated deviation defined with Eq. (10) using PC-SAFT with the generalized k_{ij} in Eqs. (15) and (16).

The solid lines in **Figure 5** and **Table 9** show the results of the PC-SAFT calculations for the isobaric solubilities of $Cr(acac)_3$ [19, 23] and $Cu(acac)_2$ [21] in $scCO_2$ as a function of temperature from 313 K to 433 K using the generalized k_{ij} obtained by Eqs. (15) and (16) as well as the predicted solubilities obtained using $k_{ij} = 0$ (dashed line). The symbols in **Figure 5** indicate the corresponding experimental data that were determined by interpolating and extrapolating from the literature values [19, 21, 23] using the spline method. As shown in **Figure 5** and **Table 9**, the isobaric solubilities of the metal precursors in $scCO_2$ can be described using the PC-SAFT calculations with the generalized k_{ij}. Consequently, we can infer that the PC-SAFT calculations using the generalized k_{ij} parameters could successfully describe the solubilities of metal precursors in $scCO_2$ over a wide temperature range, as investigated in this study. Therefore, this approach can be useful for designing the actual deposition processes based on $scCO_2$, which are generally carried out at higher temperatures.

5. Conclusions

Herein we aimed to develop a method for predicting the solubilities of two metal acetylacetonates, $Cr(acac)_3$ and $Cu(acac)_2$, in $scCO_2$ using the PC-SAFT equation of state. The solubilities of the metal precursors in various organic solvents were measured and used to determine the PC-SAFT pure-component parameters (segment number, segment diameter, and dispersion energy) for the metal precursors. The pure-component parameters of the metal precursors determined with the PC-SAFT fitting were then applied to predict the solubilities of the metal precursors in $scCO_2$ via PC-SAFT. These predictions reproduced the metal precursor solubilities over a wide range of temperatures and pressures under almost all conditions, even though the binary interaction parameter k_{ij} was set to zero in the combining rule. The solubilities in $scCO_2$ were also fit using k_{ij} as an adjustable parameter, and the temperature dependence of k_{ij} was parameterized, enabling the accurate PC-SAFT description of the isobaric solubilities of these metal precursors in $scCO_2$. On the other hand, the present method using the original PC-SAFT does not consider the contribution of the polarity of the components, including the quadrupole moment of CO_2. Consequently, a PC-SAFT approach that considers the polarity [81, 82] may improve the results of the calculated solubilities, which will be investigated in the future.

Acknowledgments

This work was supported by a JSPS (Japan Society for the Promotion of Science) KAKENHI Grant-in-Aid for Scientific Research [grant number 18K14045].

Conflicts of interest

There are no conflicts of interest to declare.

References

[1] B. Tezcan, F. Ulusal, A. Egitmen, B. Guzel, Preparation of metallic Pd nanoparticles using supercritical CO_2 deposition: An efficient catalyst for Suzuki cross-coupling reaction, J. Nanopart. Res., 20 (2018) 145. https://doi.org/10.1007/s11051-018-4252-0

[2] Y. Qiao, N. Said, M. Rauser, K. Yan, F. Qin, N. Theyssen, W. Leitner, Preparation of SBA-15 supported Pt/Pd bimetallic catalysts using supercritical fluid reactive deposition: how do solvent effects during material synthesis affect catalytic properties?, Green Chem., 19 (2017) 977-986. https://doi.org/10.1039/c6gc02490d

[3] I. Ushiki, N. Takahashi, M. Koike, Y. Sato, S. Takishima, H. Inomata, Adsorption kinetics of rhodium (III) acetylacetonate onto mesoporous silica adsorbents in the presence of supercritical carbon dioxide, J. Supercrit. Fluid., 135 (2018) 137-144. https://doi.org/10.1016/j.supflu.2018.01.017

[4] I. Ushiki, M. Koike, T. Shimizu, Y. Sato, S. Takishima, H. Inomata, Measurement and modeling of adsorption equilibria of cobalt (III) acetylacetonate on MCM-41 mesoporous silica in the presence of supercritical carbon dioxide with methanol co-solvent, J. Supercrit. Fluid., 140 (2018) 329-335. https://doi.org/10.1016/j.supflu.2018.06.015

[5] I. Ushiki, N. Takahashi, T. Shimizu, Y. Sato, M. Ota, R.L. Smith, H. Inomata, Adsorption equilibria of rhodium acetylacetonate with MCM-41, MSU-H, and HMS silica substrates in supercritical carbon dioxide for preparing catalytic mesoporous materials, J. Supercrit. Fluid., 120 (2017) 240-248. https://doi.org/10.1016/j.supflu.2016.05.032

[6] T. Shimizu, I. Ushiki, M. Ota, Y. Sato, N. Koizumi, H. Inomata, Preparation of mesoporous silica supported cobalt catalysts using supercritical fluids for Fischer-Tropsch synthesis, Chem. Eng. Res. Des., 95 (2015) 64-68. https://doi.org/10.1016/j.cherd.2015.01.005

[7] K. Matsuyama, T. Tsubaki, T. Kato, T. Okuyama, H. Muto, Preparation of catalytically active Au nanoparticles by sputter deposition and their encapsulation in metal-organic framework of $Cu_3(BTC)_2$, Mater. Lett., 261 (2020). https://doi.org/10.1016/j.matlet.2019.127124

[8] J. Morere, E. Sanchez-Miguel, M.J. Tenorio, C. Pando, A. Cabanas, Supercritical fluid preparation of Pt, Ru and Ni/graphene nanocomposites and their application as selective

catalysts in the partial hydrogenation of limonene, J. Supercrit. Fluid., 120 (2017) 7-17. https://doi.org/10.1016/j.supflu.2016.10.007

[9] K. Matsuyama, S. Tanaka, T. Kato, T. Okuyama, H. Muto, R. Miyamoto, H.-z. Bai, Supercritical fluid-assisted immobilization of Pd nanoparticles in the mesopores of hierarchical porous SiO_2 for catalytic applications, J. Supercrit. Fluid., 130 (2017) 140-146. https://doi.org/10.1016/j.supflu.2017.07.032

[10] W.T. Chiu, C.Y. Chen, T.F.M. Chang, T. Hashimoto, H. Kurosu, M. Sone, Ni-P and TiO_2 codeposition on silk textile via supercritical CO_2 promoted electroless plating for flexible and wearable photocatalytic devices, Electrochim. Acta, 294 (2019) 68-75. https://doi.org/10.1016/j.electacta.2018.10.076

[11] Q.H. Do, C.C. Zeng, Reactive Deposition of Ultrathin Conformal Vanadium Pentoxide within Carbon Nanotube Buckypaper in Supercritical Fluid CO_2 for Electrochemical Capacitor, Ind. Eng. Chem. Res., 57 (2018) 6863-6869. https://doi.org/10.1021/acs.iecr.7b04916

[12] S.B. Barim, S.E. Bozbag, H.B. Yu, R. Kizilel, M. Aindow, C. Erkey, Mesoporous carbon aerogel supported PtCu bimetallic nanoparticles via supercritical deposition and their dealloying and electrocatalytic behaviour, Catal. Today, 310 (2018) 166-175. https://doi.org/10.1016/j.cattod.2017.09.023

[13] F.E.S. Oztuna, S.B. Barim, S.E. Bozbag, H. Yu, M. Aindow, U. Unal, C. Erkey, Graphene Aerogel Supported Pt Electrocatalysts for Oxygen Reduction Reaction by Supercritical Deposition, Electrochim. Acta, 250 (2017) 174-184. https://doi.org/10.1016/j.electacta.2017.08.067

[14] W.T. Chiu, Y. Tahara, C.Y. Chen, T.F.M. Chang, T. Hashimoto, H. Kurosu, M. Sone, A Supercritical CO_2 Promoted Electroless Ni-P Plating on Silk and Their Fundamental Characteristics Investigations, J. Electrochem. Soc., 164 (2017) D406-D411. https://doi.org/10.1149/2.0551707jes

[15] Y. Zhao, K. Jung, Y. Shimoyama, Y. Shimogaki, T. Momose, Conformal Bismuth Titanate Formation Using Supercritical Fluid Deposition, Ecs J. Solid State Sci. Technol., 6 (2017) 483-488. https://doi.org/10.1149/2.0011708jss

[16] S.B. Barim, E. Uzunlar, S.E. Bozbag, C. Erkey, Review—Supercritical Deposition: A

Powerful Technique for Synthesis of Functional Materials for Electrochemical Energy Conversion and Storage, J. Electrochem. Soc., 167 (2020) 054510. https://doi.org/10.1149/1945-7111/ab68d1

[17] S.E. Bozbag, C. Erkey, Supercritical deposition: Current status and perspectives for the preparation of supported metal nanostructures, J. Supercrit. Fluid., 96 (2015) 298-312. https://doi.org/10.1016/j.supflu.2014.09.036

[18] I. Ushiki, K. Matsuyama, R.L. Smith, Chapter 15 - Sustainable Approaches for Materials Engineering With Supercritical Carbon Dioxide, in: G. Szekely, A. Livingston (Eds.) Sustainable Nanoscale Engineering, Elsevier, 2020, pp. 395-414. https://doi.org/10.1016/B978-0-12-814681-1.00015-1

[19] M. Haruki, F. Kobayashi, K. Kishimoto, S. Kihara, S. Takishima, Measurement of the solubility of metal complexes in supercritical carbon dioxide using a UV-vis spectrometer, Fluid Phase Equilib., 280 (2009) 49-55. https://doi.org/10.1016/j.fluid.2009.03.010

[20] M. Haruki, F. Kobayashi, M. Okamoto, S. Kihara, S. Takishima, Solubility of beta-diketonate complexes for cobalt(III) and chromium(III) in supercritical carbon dioxide, Fluid Phase Equilib., 297 (2010) 155-161. https://doi.org/10.1016/j.fluid.2010.02.028

[21] M. Haruki, F. Kobayashi, S. Kihara, S. Takishima, Solubility of beta-Diketonate Complexes of Copper(II) and Cobalt(II) in Supercritical Carbon Dioxide, J. Chem. Eng. Data, 56 (2011) 2230-2235. https://doi.org/10.1021/je101255v

[22] M. Haruki, F. Kobayashi, S.I. Kihara, S. Takishima, Effect of the chemical structures of iron complexes on the solubilities in supercritical carbon dioxide, Fluid Phase Equilib., 308 (2011) 1-7. https://doi.org/10.1016/j.fluid.2011.05.008

[23] M. Haruki, M. Ohara, S.-i. Kihara, S. Takishima, Solubilities of cobalt(III) and chromium(III) acetylacetonates in supercritical carbon dioxide at elevated temperatures, Fluid Phase Equilib., 357 (2013) 50-56. https://doi.org/10.1016/j.fluid.2013.02.004

[24] W.H. Teoh, R. Mammucari, N.R. Foster, Solubility of organometallic complexes in supercritical carbon dioxide: A review, J. Organomet. Chem., 724 (2013) 102-116. https://doi.org/10.1016/j.jorganchem.2012.10.005

[25] C. Erkey, Chapter 3 - Thermodynamics of Mixtures of Metal Complexes with Supercritical Fluids, in: C. Erkey (Ed.) Supercritical Fluid Science and Technology, Elsevier, Amsterdam, Netherlands, 2011, pp. 21-40. https://doi.org/10.1016/B978-0-08-045329-3.00003-2

[26] W.C. Andersen, R.E. Sievers, A.F. Lagalante, T.J. Bruno, Solubilities of Cerium(IV), Terbium(III), and Iron(III) β-Diketonates in Supercritical Carbon Dioxide, J. Chem. Eng. Data, 46 (2001) 1045-1049. https://doi.org/10.1021/je000257c

[27] O. Aschenbrenner, S. Kemper, N. Dahmen, K. Schaber, E. Dinjus, Solubility of beta-diketonates, cyclopentadienyls, and cyclooctadiene complexes with various metals in supercritical carbon dioxide, J. Supercrit. Fluid., 41 (2007) 179-186. https://doi.org/10.1016/j.supflu.2006.10.011

[28] J. Chrastil, Solubility of solids and liquids in supercritical gases, J. Phys. Chem., 86 (1982) 3016-3021. https://doi.org/10.1021/j100212a041

[29] J. Morere, M.J. Tenorio, C. Pando, J.A.R. Renuncio, A. Cabanas, Solubility of two metal-organic ruthenium precursors in supercritical CO_2 and their application in supercritical fluid technology, J. Chem. Thermodyn., 58 (2013) 55-61. https://doi.org/10.1016/j.jct.2012.09.029

[30] C.Y. Kong, K. Sone, T. Sako, T. Funazukuri, S. Kagei, Solubility determination of organometallic complexes in supercritical carbon dioxide by chromatographic impulse response method, Fluid Phase Equilib., 302 (2011) 347-353. https://doi.org/10.1016/j.fluid.2010.09.034

[31] S. Yoda, Y. Mizuno, T. Furuya, Y. Takebayashi, K. Otake, T. Tsuji, T. Hiaki, Solubility measurements of noble metal acetylacetonates in supercritical carbon dioxide by high performance liquid chromatography (HPLC), J. Supercrit. Fluid., 44 (2008) 139-147. https://doi.org/10.1016/j.supflu.2007.11.002

[32] D.Y. Peng, D.B. Robinson, A New Two-Constant Equation of State, Ind. Eng. Chem. Fundam., 15 (1976) 59-64. https://doi.org/10.1021/i160057a011

[33] M.S. Wertheim, Fluids with highly directional attractive forces. 4. Equilibrium polymerization, J. Stat. Phys., 42 (1986) 477-492. https://doi.org/10.1007/bf01127722

[34] M.S. Wertheim, Fluids with highly directional attractive forces. 3. Multiple attraction sites,

J. Stat. Phys., 42 (1986) 459-476. https://doi.org/10.1007/bf01127721

[35] M.S. Wertheim, Fluids with highly directional attractive forces. 2. Thermodynamic perturbation theory and integral equations, J. Stat. Phys., 35 (1984) 35-47. https://doi.org/10.1007/bf01017363

[36] M.S. Wertheim, Fluids with highly directional attractive forces. 1. Statistical thermodynamics, J. Stat. Phys., 35 (1984) 19-34. https://doi.org/10.1007/bf01017362

[37] J. Gross, G. Sadowski, Perturbed-Chain SAFT: An Equation of State Based on a Perturbation Theory for Chain Molecules, Ind. Eng. Chem. Res., 40 (2001) 1244-1260. https://doi.org/10.1021/ie0003887

[38] J. Gross, G. Sadowski, Application of the Perturbed-Chain SAFT Equation of State to Associating Systems, Ind. Eng. Chem. Res., 41 (2002) 5510-5515. https://doi.org/10.1021/ie010954d

[39] G. Sodeifian, S.M. Hazaveie, S.A. Sajadian, F. Razmimanesh, Experimental investigation and modeling of the solubility of oxcarbazepine (an anticonvulsant agent) in supercritical carbon dioxide, Fluid Phase Equilib., 493 (2019) 160-173. https://doi.org/10.1016/j.fluid.2019.04.013

[40] G. Sodeifian, N. Saadati Ardestani, S.A. Sajadian, H.S. Panah, Measurement, correlation and thermodynamic modeling of the solubility of Ketotifen fumarate (KTF) in supercritical carbon dioxide: Evaluation of PCP-SAFT equation of state, Fluid Phase Equilib., 458 (2018) 102-114. https://doi.org/10.1016/j.fluid.2017.11.016

[41] G. Sodeifian, F. Razmimanesh, S.A. Sajadian, H. Soltani Panah, Solubility measurement of an antihistamine drug (Loratadine) in supercritical carbon dioxide: Assessment of qCPA and PCP-SAFT equations of state, Fluid Phase Equilib., 472 (2018) 147-159. https://doi.org/10.1016/j.fluid.2018.05.018

[42] K. Gong, S.R. Panuganti, W.G. Chapman, Study of solubility and swelling ratio in polymer-CO_2 systems using the PC-SAFT equation of state, J. Appl. Polym. Sci., 134 (2017). https://doi.org/10.1002/app.44804

[43] J. Chmelař, K. Haškovcová, M. Podivinská, J. Kosek, Equilibrium Sorption of Propane

and 1-Hexene in Polyethylene: Experiments and Perturbed-Chain Statistical Associating Fluid Theory Simulations, Ind. Eng. Chem. Res., 56 (2017) 6820-6826. https://doi.org/10.1021/acs.iecr.7b00572

[44] R.I. Canales, C. Held, M.J. Lubben, J.F. Brennecke, G. Sadowski, Predicting the Solubility of CO_2 in Toluene + Ionic Liquid Mixtures with PC-SAFT, Ind. Eng. Chem. Res., 56 (2017) 9885-9894. https://doi.org/10.1021/acs.iecr.7b01497

[45] L.F. Zubeir, T. Spyriouni, D. Roest, J.R. Hill, M.C. Kroon, Effect of Oxygenation on Carbon Dioxide Absorption and Thermophysical Properties of Ionic Liquids: Experiments and Modeling Using Electrolyte PC-SAFT, Ind. Eng. Chem. Res., 55 (2016) 8869-8882. https://doi.org/10.1021/acs.iecr.6b01984

[46] C.H.J.T. Dietz, J.T. Creemers, M.A. Meuleman, C. Held, G. Sadowski, M. Van Sint Annaland, F. Gallucci, M.C. Kroon, Determination of the Total Vapor Pressure of Hydrophobic Deep Eutectic Solvents: Experiments and Perturbed-Chain Statistical Associating Fluid Theory Modeling, ACS Sustainable Chem. Eng., 7 (2019) 4047−4057. https://doi.org/10.1021/acssuschemeng.8b05449

[47] C. Dietz, F. Gallucci, M.V. Annaland, C. Held, M.C. Kroon, 110th Anniversary: Distribution Coefficients of Furfural and 5-Hydroxymethylfurfural in Hydrophobic Deep Eutectic Solvent plus Water Systems: Experiments and Perturbed-Chain Statistical Associating Fluid Theory Predictions, Ind. Eng. Chem. Res., 58 (2019) 4240-4247. https://doi.org/10.1021/acs.iecr.8b06234

[48] N.I. Diamantonis, I.G. Economou, Evaluation of Statistical Associating Fluid Theory (SAFT) and Perturbed Chain-SAFT Equations of State for the Calculation of Thermodynamic Derivative Properties of Fluids Related to Carbon Capture and Sequestration, Energy Fuels, 25 (2011) 3334-3343. https://doi.org/10.1021/ef200387p

[49] I. Ushiki, Y. Sato, S. Takishima, H. Inomata, Thermodynamic Modeling of the Solubility of Acetylacetonate-Type Metal Precursors in Supercritical Carbon Dioxide Using the PC-SAFT Equation of State, J. Chem. Eng. Jpn, 52 (2019) 243-252. https://doi.org/10.1252/jcej.18we194

[50] R. Paus, Y. Ji, L. Vahle, G. Sadowski, Predicting the Solubility Advantage of Amorphous

Pharmaceuticals: A Novel Thermodynamic Approach, Mol. Pharmaceutics, 12 (2015) 2823-2833. https://doi.org/10.1021/mp500824d

[51] F. Ruether, G. Sadowski, Modeling the solubility of pharmaceuticals in pure solvents and solvent mixtures for drug process design, J. Pharm. Sci., 98 (2009) 4205-4215. https://doi.org/10.1002/jps.21725

[52] R. Paus, E. Hart, Y. Ji, G. Sadowski, Solubility and Caloric Properties of Cinnarizine, J. Chem. Eng. Data, 60 (2015) 2256-2261. https://doi.org/10.1021/acs.jced.5b00075

[53] Saturated Liquid Density Calculation by DIPPR105 Equation, DDBST GmbH, accessed Apr 20, 2020. http://ddbonline.ddbst.de/DIPPR105DensityCalculation/DIPPR105CalculationCGI.exe

[54] NIST, NIST Chemistry WebBook, NIST Standard Reference Database Number 69, National Institute of Standards and Technology, Gaithersburg, MD, 2019.

[55] Z. Zou, L. Dang, P. Liu, H. Wei, Solubility of Fluorene in Different Solvents from 278.98 K to 338.35 K, J. Chem. Eng. Data, 52 (2007) 1501-1502. https://doi.org/10.1021/je700179q

[56] Y. Han, Z. Wang, Solubility of Fluorene in Benzene, Chloroform, Acetone, 1-Propanol, Isobutanol, and Methylbenzene from (283 to 323) K, J. Chem. Eng. Data, 54 (2009) 148-149. https://doi.org/10.1021/je800676s

[57] A. Shayanfar, S.H. Eghrary, F. Sardari, W.E. Acree, A. Jouyban, Solubility of Anthracene and Phenanthrene in Ethanol + 2,2,4-Trimethylpentane Mixtures at Different Temperatures, J. Chem. Eng. Data, 56 (2011) 2290-2294. https://doi.org/10.1021/je101272u

[58] L.E. Roy, C.E. HernÁandez, W.E. Acree, Thermodynamics of Mobile Order Theory. Part 3. Comparison of Experimental and Predicted Solubilities for Fluoranthene and Pyrene, Polycyclic Aromat. Compd., 13 (1999) 205-219. https://doi.org/10.1080/10406639908020564

[59] J.B.G. Daldrup, C. Held, F. Ruether, G. Schembecker, G. Sadowski, Measurement and modeling solubility of aqueous multisolute amino-acid solutions, Ind. Eng. Chem. Res., 49 (2010) 1395-1401. https://doi.org/10.1021/ie900913c

[60] Y. Zhang, W. Jian, Y. Song, W. Liu, M. Yang, J. Zhao, Y. Liu, Y. Zhao, (p, ρ, T) Behavior

of CO_2 + Tetradecane Systems: Experiments and Thermodynamic Modeling, J. Chem. Eng. Data, 60 (2015) 1476-1486. https://doi.org/10.1021/acs.jced.5b00049

[61] B.S. Shin, W.G. Rho, S.-S. You, J.W. Kang, C.S. Lee, Evaluation of Thermodynamic Models for Predicting Phase Equilibria of CO_2 + Impurity Binary Mixture, Int. J. Thermophys., 39 (2018) 44. https://doi.org/10.1007/s10765-018-2364-5

[62] M. Aghaie, N. Rezaei, S. Zendehboudi, Assessment of carbon dioxide solubility in ionic liquid/toluene/water systems by extended PR and PC-SAFT EOSs: Carbon capture implication, Journal of Molecular Liquids, 275 (2019) 323-337. https://doi.org/10.1016/j.molliq.2018.11.038

[63] Y. Song, W. Jian, Y. Zhang, M. Yang, J. Zhao, W. Liu, Y. Liu, Y. Shen, Density Measurement and PC-SAFT/tPC-PSAFT Modeling of the CO_2 + H_2O System over a Wide Temperature Range, J. Chem. Eng. Data, 59 (2014) 1400-1410. https://doi.org/10.1021/je500062a

[64] F. Tumakaka, G. Sadowski, Application of the Perturbed-Chain SAFT equation of state to polar systems, Fluid Phase Equilib., 217 (2004) 233-239. https://doi.org/10.1016/j.fluid.2002.12.002

[65] G.M. Kontogeorgis, G.K. Folas, Thermodynamic Models for Industrial Applications: From Classical and Advanced Mixing Rules to Association Theories, John Wiley & Sons, Chichester, U.K., 2009. https://doi.org/10.1002/9780470747537

[66] J.M. Prausnitz, R.N. Lichtentaler, E.G. de Azevedo, Molecular Thermodynamics of Fluid-Phase Equilibria, 3rd Edition, Prentice Hall, Upper saddle river, New Jersey, 1998.

[67] T. Spyriouni, X. Krokidis, I.G. Economou, Thermodynamics of pharmaceuticals: Prediction of solubility in pure and mixed solvents with PC-SAFT, Fluid Phase Equilib., 302 (2011) 331-337. https://doi.org/10.1016/j.fluid.2010.08.029

[68] J. Brinkmann, C. Luebbert, D.H. Zaitsau, S.P. Verevkin, G. Sadowski, Thermodynamic Modeling of Triglycerides using PC-SAFT, J. Chem. Eng. Data, 64 (2019) 1446-1453. https://doi.org/10.1021/acs.jced.8b01046

[69] H.B. Rose, T. Greinert, C. Held, G. Sadowski, A.S. Bommarius, Mutual Influence of

Furfural and Furancarboxylic Acids on Their Solubility in Aqueous Solutions: Experiments and Perturbed-Chain Statistical Associating Fluid Theory (PC-SAFT) Predictions, J. Chem. Eng. Data, 63 (2018) 1460-1470. https://doi.org/10.1021/acs.jced.7b01039

[70] C. Dietz, A. Erve, M.C. Kroon, M.V. Annaland, F. Gallucci, C. Held, Thermodynamic properties of hydrophobic deep eutectic solvents and solubility of water and HMF in them: Measurements and PC-SAFT modeling, Fluid Phase Equilib., 489 (2019) 75-82. https://doi.org/10.1016/j.fluid.2019.02.010

[71] H.T. Do, Y.Z. Chua, J. Habicht, M. Klinksiek, M. Hallermann, D. Zaitsau, C. Schick, C. Held, Melting properties of peptides and their solubility in water. Part 1: dipeptides based on glycine or alanine, RSC Adv., 9 (2019) 32722-32734. https://doi.org/10.1039/C9RA05730G

[72] S. Poston, A. Reisman, Density determination of silver neodecanoate, tungsten hexacarbonyl, and a series of metal acetylacetonates and hexafluoroacetylacetonates, J. Electron. Mater., 18 (1989) 79-84. https://doi.org/10.1007/BF02655348

[73] V.G. Minkina, Initial compounds for obtaining high-temperature superconducting films by the CVD-method, Russ. Chem. Bull., 42 (1993) 1460-1466. https://doi.org/10.1007/BF00699173

[74] A.C. Galvao, P.F. Arce, W.S. Robazza, T.D. Machado, C.A.L. Franca, Solubility and Pseudo Polymorphic Behavior of Nicotinic Acid in Alcoholic Solutions: Experimental Data and Phase Equilibrium Modeling, Ind. Eng. Chem. Res., 59 (2020) 1319-1326. https://doi.org/10.1021/acs.iecr.9b05367

[75] G. Sodeifian, S.A. Sajadian, R. Derakhsheshpour, Experimental measurement and thermodynamic modeling of Lansoprazole solubility in supercritical carbon dioxide: Application of SAFT-VR EoS, Fluid Phase Equilib., 507 (2020) 112422. https://doi.org/10.1016/j.fluid.2019.112422

[76] B.E. Poling, J.M. Prausnitz, J.P. O'Connell, The Properties of Gases and Liquids, 5 ed., McGraw-Hill, New York, US, 2000.

[77] P.P. Semyannikov, I.K. Igumenov, S.V. Trubin, T.P. Chusova, Z.I. Semenova, Thermodynamics of chromium acetylacetonate sublimation, Thermochim. Acta, 432 (2005) 91-98. https://doi.org/10.1016/j.tca.2005.02.034

[78] N.B. Morozova, G.I. Zharkova, P.P. Semyannikov, S.V. Sysoev, I.K. Igumenov, N.E. Fedotova, N.V. Gelfond, Vapor pressure of precursors for CVD on the base of platinum group metals, J. De Phys. IV, 11 (2001) 609-616. https://doi.org/10.1051/jp4:2001377

[79] Y. Zhang, S. Wei, H.-H. Wang, J.-Q. Liu, W. Wang, Solubility Measurement and the Correlation of 1-Naphthaleneacetic Acid in Pure and Methanol + Water Binary Solvents from T = (278.25 to 323.55) K, J. Chem. Eng. Data, 62 (2017) 1292-1301. https://doi.org/10.1021/acs.jced.6b00816

[80] R. Span, W. Wagner, A New Equation of State for Carbon Dioxide Covering the Fluid Region from the Triple-Point Temperature to 1100 K at Pressures up to 800 MPa, J. Phys. Chem. Ref. Data, 25 (1996) 1509-1596. https://doi.org/10.1063/1.555991

[81] J. Gross, J. Vrabec, An equation-of-state contribution for polar components: Dipolar molecules, AlChE J., 52 (2006) 1194-1204. https://doi.org/10.1002/aic.10683

[82] J. Gross, An equation-of-state contribution for polar components: Quadrupolar molecules, AlChE J., 51 (2005) 2556-2568. https://doi.org/10.1002/aic.10502